

Efficient force field and energy emulation through partition of permutationally equivalent atoms

Hao Li,¹ Musen Zhou,² Jessalyn Sebastian,¹ Jianzhong Wu,² and Mengyang Gu^{1, a)}

¹⁾Department of Statistics and Applied Probability, University of California, Santa Barbara, CA 93106, USA

²⁾Department of Chemical and Environmental Engineering, University of California, Riverside, CA 92521, USA

(Dated: 16 February 2022)

Gaussian process (GP) emulator has been used as a surrogate model for predicting force field and molecular potential, to overcome the computational bottleneck of molecular dynamics simulation. Integrating both atomic force and energy in predictions was found to be more accurate than using energy alone, yet it requires $O((NM)^3)$ computational operations for computing the likelihood function and making predictions, where N is the number of atoms and M is the number of simulated configurations in the training sample, due to the inversion of a large covariance matrix. The large computational need limits its applications to emulating simulation of small molecules. The computational challenge of using both gradient information and function values in GPs was recently noticed in statistics and machine learning communities, where conventional approximation methods, such as the low rank decomposition or sparse approximation, may not work well. Here we introduce a new approach, the atomized force field (AFF) model, that integrates both force and energy in the emulator with many fewer computational operations. The drastic reduction on computation is achieved by utilizing the naturally sparse structure of the covariance satisfying the constraints of the energy conservation and permutation symmetry of atoms. The efficient machine learning algorithm extends the limits of its applications on larger molecules under the same computational budget, with nearly no loss of predictive accuracy. Furthermore, our approach contains uncertainty assessment of predictions of atomic forces and potentials, useful for developing a sequential design over the chemical input space, with almost no increase in computational cost.

I. INTRODUCTION

Fast and accurate emulation of atomic forces and energy is essential to access the microscopic details of chemical and biological events via molecular simulation. Classical molecular dynamics (cMD) relies on a pre-defined force field with semi-empirical forms of the potential energy which often lacks accuracy, while *ab initio* MD (AIMD) sacrifices computational efficiency for a higher level of accuracy. In principle, machine learning (ML) approaches can provide a surrogate model to achieve both accuracy and computational efficiency at the levels of AIMD and cMD, thus providing new applications that would not be achievable with conventional methods. While recent years have witnessed enormous development of ML potentials, the field is still rapidly evolving, as many theoretical and computational issues remain to be addressed for the efficient representation of potential-energy surfaces to extend the limits of machine learning tools on large-scale simulation from electronic structure calculations.

Our essential task is to efficiently learn the map between the molecule-level information, such as potential energy surface and atomic forces, and atomic coordinates. Deep neural network (DNN) and Gaussian process

(GP) that encodes physical symmetries are popular tools to emulate AIMD simulation containing a large number of single atoms or small molecules (such as H_2O)^{1–3}. Some effective machine learning approaches have been developed to emulate the dynamics of molecules containing a larger number atoms with different types. The kernel ridge regression (KRR) approach based on pairwise diatomic positions and nuclear charge, for instance, was proposed to emulate potential energies of organic molecules⁴. Prediction by KRR is equivalent to using the predictive mean in Gaussian process regression (GPR)⁵, whereas the uncertainty of predictions can be assessed without additional cost in a GPR. The Gaussian approximation potential framework (GAP)⁶, as another example, approximates the total energy functional through a decomposition of local atomic energy functional by using self-designed atomic neighborhood information. This approach is often used along with the smooth overlap of atomic positions (SOAP)¹ to measure the local atomic neighborhood information, such that predictions satisfy translational, permutational and rotational symmetries of atoms, where the the inducing point sparse approximation⁷ is often used to improve computational scalability. DNN architectures were also developed to emulate molecular dynamics simulations⁸, where a large number of training samples were often used to achieve highly accurate predictive performance. The GP typically requires fewer samples for accurate predictions, as the closed-form expression of the predictions is available in a GP model, whereas DNN typically relies on numer-

^{a)}Author to whom correspondence should be addressed: mengyang@pstat.ucsb.edu

ical optimization in a large parameter space.

When the number and the types of atoms in a molecule become large, predictions by GPR or DNN become less accurate. It was recently found that combining force and energy samples with energy conservation constraints can improve the predictive accuracy of atomic forces and potential energies in AIMD simulation^{9–13}. The approach, called gradient-domain machine learning (GDML)⁹, starts with the principle of the conservation of energy, where the force on each atom $\mathbf{F}_i(\mathbf{x})$ is related to the potential energy $E(\mathbf{x})$

$$\mathbf{F}_i(\mathbf{x}) = -\nabla_{\mathbf{r}_i} E(\mathbf{x}), \quad (1)$$

where $\mathbf{x} = [\mathbf{r}_1, \mathbf{r}_2, \dots, \mathbf{r}_N]$ is a $3 \times N$ matrix of atomic Cartesian coordinates for a system with N atoms, and \mathbf{r}_i denotes the 3D coordinates for each atom. The pairwise inverse distance of atom positions were often used to construct the descriptor $\mathbf{D}(\mathbf{x})$ of a molecule

$$\mathbf{D}(\mathbf{x})_{ij} = \begin{cases} \|\mathbf{r}_i - \mathbf{r}_j\|^{-1} & \text{for } i > j, \\ 0 & \text{o.w.}, \end{cases} \quad (2)$$

where $\|\cdot\|$ denotes the Euclidean distance. The similarity of potential energies between two molecules with atom positions \mathbf{x}_a and \mathbf{x}_b can be expressed by a kernel function $K(\mathbf{D}(\mathbf{x}_a), \mathbf{D}(\mathbf{x}_b))$. The $3N \times 3N$ covariance matrix of atomic forces can be denoted by $\mathbf{R}(\mathbf{x}_a, \mathbf{x}_b)$, where the (i, j) element is $(\mathbf{R}(\mathbf{x}_a, \mathbf{x}_b))_{ij} = \nabla_{\mathbf{r}_{ai}} K(\mathbf{D}(\mathbf{x}_a), \mathbf{D}(\mathbf{x}_b)) \nabla_{\mathbf{r}_{bj}}^T$, because of energy conservation in Equ. (1). Given M configurations of a molecule, each containing N atoms, parameter estimation and predictions of the atomic forces by the GDML approach⁹ and its symmetric version¹⁴ involve constructing and inverting a $3NM \times 3NM$ Hessian covariance matrix. The computational cost of constructing this covariance matrix scales as $\mathcal{O}(M^2 N^3)$ and the cost of its inversion scales as $\mathcal{O}(M^3 N^3)$, both increasing rapidly along with the number of atoms or the number of available simulation runs to train a surrogate model. The immense computational complexity of the surrogate model limits its application to predicting forces in the simulation of molecules with a small number of atoms and training sample size. The computational bottleneck limits the applications in energy prediction to single molecules with approximately 20 atoms or less. For molecules with more atoms or systems with multiple molecules, a faster approach is needed to bypass the computational bottleneck in simulation and emulation.

A wide range of approximation methods for alleviating the computational cost of GP models have been proposed in recent years, including, for instance, the induced point approach^{7,15}, low rank approximation¹⁶, covariance tapering¹⁷, hierarchical nearest neighbor methods¹⁸, stochastic partial differential equation approach^{19,20}, local Gaussian process approach²¹ and periodic embedding²². Though these methods have been shown to be useful for approximating GP models with observations at a low dimensional

input space, none of these methods focuses on approximating GP models with high-dimensional gradient observations. Here the atomic force vectors are the gradient observations of the systems. Incorporating the gradient information into GP is also critically important in many other applications, such as Bayesian optimization for inverse design²³. However, the large computational cost prevents the direct applications of GP models with high-dimensional gradient information in large-scale systems, a problem which was recently realized in the statistics and machine learning communities²⁴. Low rank approximation and sparse approximation of the covariance were studied²⁵, yet the predictive accuracy can be degraded. The recent approach²⁴ reduces the computational complexity for GP with gradient observations with respect to the dimension of gradients, but the method requires $\mathcal{O}(M^6)$ computational operations, which is prohibitive for moderately large training runs M . Surprisingly, we found that our covariance matrix of the atomic forces is approximately sparse, when we enforce energy conservation and permutation symmetry of atoms onto the covariance function. This property can be used to improve computational operations substantially, yet without reducing the accuracy in predictions.

In this work, we propose a new surrogate model called the atomized force field (AFF) emulator for emulating the atomic force and energy in AIMD simulations, which reduces the computational operations from inverting enormous correlation matrix of atomic force vectors, whereas maintaining high predictive accuracy. Unlike other sparse GP approximation, the AFF method reduces the computation complexity of GP with derivatives without sacrificing predictive accuracy, as many terms in the covariance is already close to zero. We outline three features of the proposed approach. First, we partition the atoms into permutationally equivalent (PE) atom sets (formally defined later), where the correlation of atomic forces at different atom sets is found to be almost negligible. Thus, we can decompose the large covariance matrix of the simulated force vectors into small sub-covariance matrices for each permutationally distinguishable atom, where the sub-covariance contains the most information in parameter estimation and predictions. This feature reduces computational operations in matrix inversion from $\mathcal{O}(N^3 M^3)$ in the GDML approach⁹ to $\mathcal{O}(NM^3)$ in the AFF model. Second, inspired by the popular induced input approach in approximating Gaussian processes^{7,15}, we develop a new model that approximates the prediction of potential energy based on simulated energy and force observations that are strongly correlated to this molecular configuration, which reduces computational operations in emulating potential energy surface. For molecules without permutational symmetries, the total computational cost for emulating forces and the potential energy required in constructing the covariance matrix in the AFF model is $\mathcal{O}(M^2 N^2)$, and in computing the likelihood and predictions is $\mathcal{O}(M^3 N)$, which is much smaller than the $\mathcal{O}(M^3 N^3)$ computational

operations required in the GDML approach⁹. Compared to some recent DNN approaches, the AFF model requires much fewer samples, typically ranging from a few hundred to a thousand, to achieve high accuracy in predictions, which makes it an attractive approach for emulating computationally expensive AIMD simulations. Finally, our model gives both predictions and uncertainty quantification, as any quantile of the predictive distribution has a closed-form expression. Quantifying the uncertainty in predictions is critically important in an inverse problem, such as optimizing molecular structures based on constraints of physical properties. Based on these new features, we are able to accurately predict atomic force vectors and the potential energy from simulation for molecules with more atoms given the same computational budget. For instance, we are able to accurately emulate the simulation of molecules with around 50 atoms from AIMD simulation within only tens of seconds in a desktop computer, as well as quantifying the uncertainties for both the predicted forces and energy.

Although the AFF model is motivated by physically informed sparse structure in the covariance matrix for simplifying computations, the model maintains some key physical ingredients of the more computationally intensive approaches, such as the GDML approach and its variants^{9,10}. The kernel function of force vectors in both GDML and AFF models, for instance, is the same, and it was derived by the conservation of energy in Equ. (1), yet the AFF model is much faster, as it utilizes a natural sparse structure in covariance found in this work. Predictions of each atom in the AFF model depend on the information of all other atoms in a molecular configuration, expressed as the pairwise distance of atoms positions. Thus, our approach should not be interpreted as a conventional method to capture local atomic information, because the descriptor used in any atomic force still incorporates the pairwise distance for all atoms. Empirical results of various examples show that our method is more efficient and more accurate than the alternatives based on the same held-out data set.

The rest of the article is organized as follows. We first present the motivation of the AFF method in Sec. II. The formal definition of PE atoms and an algorithm to find PE atom sets are introduced in Sec. II A. In Sec. II B, we give a detailed introduction of the AFF framework on force prediction. Then, in Sec. II C, we discuss the details of our approach to energy prediction. Finally, in Sec. III, we apply our method to emulate atomic force vectors and potential energy in *ab initio* simulation, and demonstrate that our approach provides higher predictive accuracy and reliable uncertainty assessment compared to other widely used methods. The conclusion of this study and potentially research directions are provided in Sec. IV.

II. METHODOLOGY

Let us consider a molecule with N atoms and denote the atomic coordinates of two configurations of this molecule as \mathbf{x}_a and \mathbf{x}_b . Assume that the vectorized descriptors $\mathbf{D}(\mathbf{x}_a)$ and $\mathbf{D}(\mathbf{x}_b)$ are used as input variables, and the correlation of the potential energy of the two configurations of this molecule is encoded by a kernel function, denoted as $K(\mathbf{D}(\mathbf{x}_a), \mathbf{D}(\mathbf{x}_b))$, where the explicit form of the kernel function is discussed in Sec. II B. By applying the connection between potential energy and force vectors in Equ. (1), the $3N \times 3N$ Hessian covariance matrix of atomic forces, denoted as $\mathbf{R}(\mathbf{x}_a, \mathbf{x}_b)$, has the (i, j) th element $(\mathbf{R}(\mathbf{x}_a, \mathbf{x}_b))_{ij} = \nabla_{\mathbf{r}_{ai}} K(\mathbf{D}(\mathbf{x}_a), \mathbf{D}(\mathbf{x}_b)) \nabla_{\mathbf{r}_{bj}}^T$, where \mathbf{r}_{ai} and \mathbf{r}_{bj} denote the i th column of \mathbf{x}_a and the j th column of \mathbf{x}_b . Each term of the Hessian covariance matrix $\mathbf{R}(\mathbf{x}_a, \mathbf{x}_b)$ can be written explicitly by the chain rule as shown in Appendix A).

Part (b) in Fig. 1 gives the empirical covariance for force vectors of three configurations of uracil in the MD17 dataset⁹. Note that the correlation between the force vectors of the same atom in three simulations is relatively large, whereas the correlation of force vectors between different atoms is close to zero, which coincides with mathematical results shown in Appendix A. Since the correlation between atomic forces on different atoms of uracil is small, we can construct separate emulators of force vectors based on the sub-covariance matrix of force vectors of the same atom in different configurations. The computational cost of this approach is much smaller than the GDML approach, as we decompose the $NM \times NM$ covariance matrix to N matrices each having dimensions $M \times M$, reducing the computational cost of inversion from $\mathcal{O}(N^3M^3)$ to $\mathcal{O}(NM^3)$, for a training dataset that contains M runs each having N atoms. Thus our approach is much more computationally efficient than GP methods using the atomic force but without utilizing the sparse structure. Note that here we have almost no loss of information, as the covariance naturally induces a sparse structure, which differs from other methods to create a sparse structure to approximate the original covariance matrix⁷. As will be seen from numerical comparison in Sec. III, our approach is more computationally scalable than the GDML approach and its symmetric variant^{9,10}, and thus our approach can be applied to predicting atomic forces and energies of molecules with many more atoms. Compared with the induced point sparse approximation⁷, our approach is an order of magnitude more accurate in terms of out of sample predictive error, shown in the supplementary materials.

Another advantage of our approach comes from incorporating the physical symmetries into the emulator, resulting in superior predictive accuracy. Atoms in a molecule may rotate or switch positions when recorded in simulation, so emulators that encode physical symmetry information can achieve higher predictive accuracy^{1,10,26–28}. The covariance function of force vec-

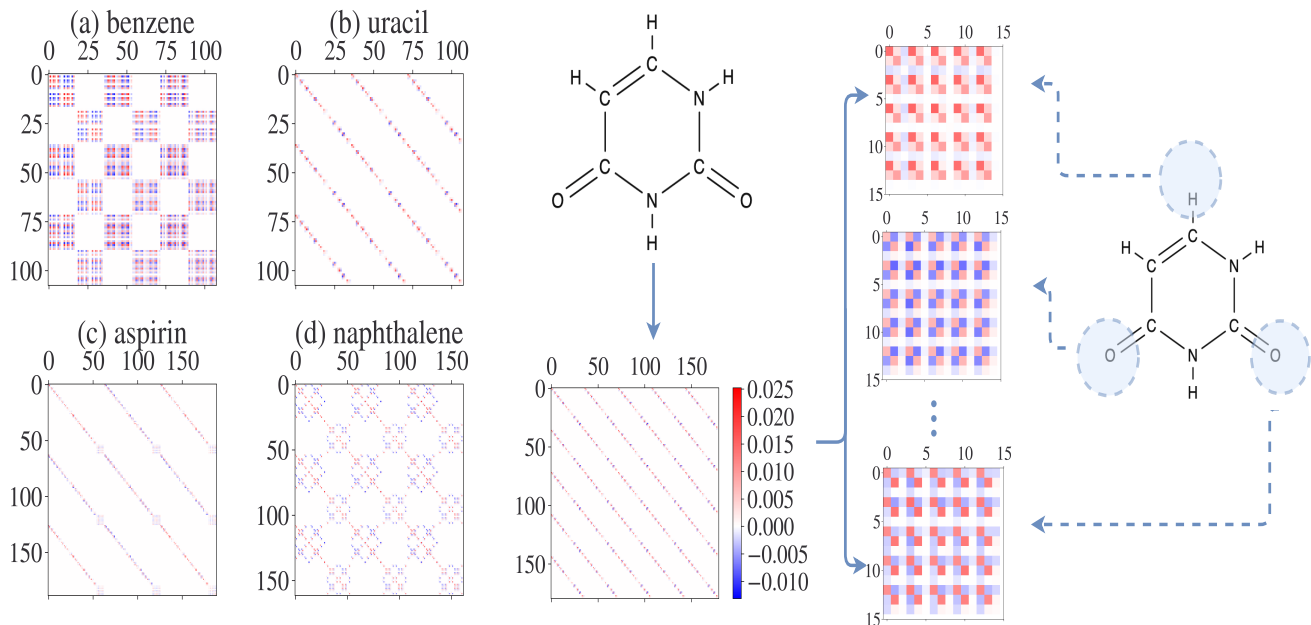


FIG. 1. Covariance structure between atomic forces and motivation for efficient computation in AFF. Displayed on the left are permutationally symmetric covariance matrices of atomic forces on 3 simulated configurations for (a) benzene, (b) uracil, (c) aspirin and (d) naphthalene. Lighter colors indicate a smaller absolute covariance, so it is clear from the figure that most elements in these matrices are near-zero. The right side of the figure shows covariance matrices of atoms in the AFF method on uracil, a molecule for which each atom is its own PE set. Here there is large correlation between atomic force on the same atom at different configurations, but very small correlation between different atoms at the same or different configurations. The rightmost part of the figure shows the subcovariance matrix of atomic force of each atom in uracil across 5 simulated configurations.

tors in the symmetric GDML (sGDML) approach¹⁰, for example, was an improved version compared to GDML, as it took the permutational symmetry of atoms into consideration. Here we use a similar approach to find the permutational symmetry, and then we extend it to define the PE groups of atoms. We found a few PE groups for molecules such as benzene, aspirin and naphthalene, in the MD17 dataset⁹. After grouping these PE atoms and parameterizing the covariance by the permutationally symmetric kernel function (formally defined in Sec. IIA), we were able to capture the large absolute covariance between these atoms. This feature empirically improves the predictive accuracy, as will be shown in Sec. III.

The key idea of the new approach, called the atomized force field emulator, is to partition atoms into different PE groups and to encode large correlation between force vectors of PE atoms at different configurations into the model. The descriptors of each atom still contain the information from all other atoms in this configuration. Thus, our approach is not to approximate the local structure of atoms; rather, it is to maintain only the non-negligible elements in the Hessian covariance matrix across different configurations in the training sample to reduce computational challenges in emulation. In the next subsection, we introduce the idea of partitioning

the atomic space to obtain PE subsets of atoms.

A. Permutationally equivalent set

We first define a group of atoms to be permutationally equivalent if they are interchangeable through any permutational operation. We call atoms from different PE sets permutationally distinct atoms. The AFF approach predicts the force of an atom in a molecule based on force from its PE group of atoms rather than all atoms in this molecule. Fig. 1 indicates that we may not need to include all atoms in a large covariance matrix for predicting atomic force to achieve computational efficiency in emulation, as many elements in the Hessian kernel matrix are near-zero.

Note that the force of an atom is expected to be similar to other atoms in its PE atom set, and the similarity can be captured by correlation in the model. For example, all four hydrogen atoms in methane (CH_4) form one set of PE atoms, while the carbon atom itself is another PE set, as the coordinates of all hydrogen atoms are interchangeable among all permutation symmetries. Benzene (C_6H_6), as another example, is comprised of just two sets of PE atoms—the first PE set containing the six carbon atoms and the second PE set containing the six hydrogen

atoms. By contrast, all twelve atoms in a uracil molecule ($C_4H_4N_2O_2$) are permutationally unique, which leads to twelve PE atom sets in uracil.

PE sets of atoms can be found by minimizing the loss function through the permutation matrix $\mathbf{P}^{*14,29}$

$$\mathbf{P}^* = \arg \min_{\mathbf{P}} \|\mathbf{P}\mathbf{A}_H\mathbf{P}^T - \mathbf{A}_G\|, \quad (3)$$

where \mathbf{A}_H and \mathbf{A}_G are adjacency matrices of two isomorphic molecules, and $(\mathbf{A})_{ij} = \|\mathbf{r}_i - \mathbf{r}_j\|$. By analyzing the index location from the permutation matrices of all permutation symmetries on the same type of molecule, we can partition atoms of molecule into sets of PE atoms $S^i = \{\mathbf{r}_1^i, \dots, \mathbf{r}_{l_i}^i\}$, where $\mathbf{r}_1^i, \dots, \mathbf{r}_{l_i}^i$ are atoms belonging to the i_{th} atom set, for $i = 1, \dots, L$.

Note that the atom in a PE set may exchange positions (e.g. through rotation) and thus the force may be recorded in different order in simulation. The Euclidean distance of the inverse pairwise distance descriptor in Equ. (2) cannot capture the similarity between two atom forces in this scenario. To represent the large similarity (correlation) between force of atoms in a PE set, one may permute the positions of atoms, through a permutationally symmetric (PS) kernel function proposed in¹⁴:

$$K_{sym}(\mathbf{D}(\mathbf{x}_a), \mathbf{D}(\mathbf{x}_b)) = \frac{1}{S^2} \sum_{p=1}^S \sum_{q=1}^S K(\mathbf{D}(\mathbf{P}_p^* \mathbf{x}_a), \mathbf{D}(\mathbf{P}_q^* \mathbf{x}_b)), \quad (4)$$

where S is the number of permutation symmetries found by Equ. (3), and \mathbf{P}_p^* is the permutation matrix of p_{th} permutation symmetry. Note that for molecule like uracil, where no permutation symmetry exists, we have $S = 1$ and $\mathbf{P}_1^* = \mathbf{I}_N$, and the kernel reduces to a conventional Hessian kernel. The correlation between the i_{th} atom of \mathbf{x}_a and the j_{th} atom of \mathbf{x}_b using the PS kernel function are the average of Hessian covariance matrix $(\mathbf{R}(\mathbf{P}_p^* \mathbf{x}_a, \mathbf{P}_q^* \mathbf{x}_b))_{ij}$, where $p = 1, \dots, S$, and $q = 1, \dots, S$.

As shown in Fig. 1 (a) and (d), as rotational symmetries were found by Equ. (3), the absolute correlation between the atoms in a PE set by the PS kernel in Equ. (4), is much larger than zero. We found that grouping the PE atoms and using all PE atoms significantly improves the predictive accuracy of atomic forces, compared with the approach that groups each atom as one set. This result is sensible as forces of PE atoms are similar, and the correlation of forces from the PS kernel between PE atoms can capture their similarity. In contrast, the conventional Hessian kernel does not encode the permutational symmetries into the model.

As mentioned before, the sGDML approach¹⁰ groups all atoms into one set for prediction, and thus the computational cost is high, as it conditions on all atoms in all simulated configurations. Note that the correlation of force between atoms from different PE sets is close to zero, compared to the correlation between atoms from the same PE set. This feature allows us to define a marginal

model of forces of atoms in each PE separately, which substantially reduces the computational complexity.

B. Atomized force field model

Consider a molecule that has N atoms grouped into L PE atom sets, each set containing l_i atoms, for $i = 1, \dots, L$. To avoid inverting the $3MN \times 3MN$ covariance matrix to compute the predictive distribution required in GDML and sGDML approaches, we decompose the large covariance matrix to construct predictive models for each PE atom set in parallel. Let $\mathbf{X} = \{\mathbf{x}_1, \dots, \mathbf{x}_M\}$ be M configurations of this model that have been simulated before (henceforth, training configurations), and let \mathbf{x}_j^i be a $3 \times l_i$ matrix that contains the i_{th} PE set's atomic coordinates in \mathbf{x}_j . Denote the forces of the atoms of i_{th} PE set in M training configurations by a $3Ml_i$ vector $\mathbf{F}_i = (\mathbf{F}_i(\mathbf{D}(\mathbf{x}_1))^T, \dots, \mathbf{F}_i(\mathbf{D}(\mathbf{x}_M))^T)^T$, where $\mathbf{F}_i(\mathbf{D}(\mathbf{x}_j))$ is a $3l_i$ atomic force vector of the i_{th} PE set at the j_{th} training configuration.

For a new molecular configuration \mathbf{x}^* , the KRR estimator minimizes the loss function that penalizes both squared error fitting loss, and the complexity of the latent function simultaneous³⁰, leading to an weighted average of the force vectors at M training configurations:

$$\hat{\mathbf{F}}_i(\mathbf{D}(\mathbf{x}^*)) = \omega_i^* \mathbf{F}_i, \quad (5)$$

where the weights follow $\omega_i^* = \mathbf{R}_{\mathbf{x}^*}^T (\mathbf{R} + \lambda \mathbf{I}_{3Ml_i})^{-1}$ with \mathbf{I}_{3Ml_i} is an identity matrix of size $3Ml_i \times 3Ml_i$. Here \mathbf{R} is a $3Ml_i \times 3Ml_i$ covariance matrix with the (j,k) -th $3l_i \times 3l_i$ block term being the Hessian matrix of the kernel function $\nabla_{\mathbf{x}_j^i} K(\mathbf{D}(\mathbf{x}_j), \mathbf{D}(\mathbf{x}_k)) \nabla_{\mathbf{x}_k^i}^T$; λ is an estimated regularization parameter; $\mathbf{R}_{\mathbf{x}^*}$ is a $3Ml_i \times 3l_i$ matrix, where the j_{th} $3l_i \times 3l_i$ block term is $\nabla_{\mathbf{x}_j^i} K(\mathbf{D}(\mathbf{x}_j), \mathbf{D}(\mathbf{x}^*)) \nabla_{\mathbf{x}^*}^T$. Note that the KRR estimator in Equ. (5) is the predictive mean of a Gaussian process regression model^{30,31}. In addition to a point estimator for predictive the untested run, the GP model also provides uncertainty assessment of the predictions, as any quantiles and intervals of predictions have a closed-form expression. Thus, we will construct a GP model for predictions and uncertainty assessments in this work.

For each PE atom set, we construct a GP model for approximating expensive simulation of force in parallel. For any M input set $\mathbf{X} = \{\mathbf{x}_1, \dots, \mathbf{x}_M\}$, the marginal distribution of the force vector \mathbf{F}_i follows a multivariate normal distribution:

$$(\mathbf{F}_i | \mathbf{R}, \sigma_i^2, \lambda) \sim \mathcal{MN}(\mathbf{0}, \sigma_i^2(\mathbf{R} + \lambda \mathbf{I}_{3Ml_i})), \quad (6)$$

for $i = 1, \dots, L$, where σ_i^2 is a variance parameter for the i_{th} PE set, and λ is the nugget parameter shared across all PE sets. Let us assume the variance parameter σ_i^2 can differ across different PE sets, as the scale of the force can vary significantly for atoms in each PE atom set, especially for those atoms of different types.

The range and nugget parameter are assumed to be the same across different PE atom sets, as the smoothness of the latent function that maps atoms' positions to forces are approximately the same across different atom sets. The computational complexity of the predictive mean in a GP emulator with the same kernel and nugget parameters across atom sets is smaller than the GP emulator with different parameters³². Similar assumptions were used in constructing the parallel partial Gaussian process emulator for emulating computationally expensive computer simulations on massive spatial coordinates for geophysical applications³².

The power exponential covariance and the Matérn covariance function are widely used as the covariance function in GP emulator³⁰. The Matérn kernel function with roughness parameter 5/2 is used as default covariance function of a few GP emulator packages^{33,34}, as well as the GDML approach for energy-conserving force field emulation⁹, as the sample path of the process is twice differentiable, leading to relatively accurate predictions for both rough and smooth functional data. Here we also use the Matérn kernel function with roughness parameter 5/2 to define the kernel function:

$$K(\mathbf{D}(\mathbf{x}_a), \mathbf{D}(\mathbf{x}_b)) = \left(1 + \sqrt{5}\frac{d}{\gamma} + \frac{5d^2}{3\gamma^2}\right) \exp\left(-\sqrt{5}\frac{d}{\gamma}\right), \quad (7)$$

where γ is the range parameter, and d is the Euclidean distance between the vectorized descriptors $\mathbf{D}(\mathbf{x}_a)$ and $\mathbf{D}(\mathbf{x}_b)$. Similar to the adjustment of kernel function used in the sGDML approach¹⁰, we transform the Matérn kernel to the PS kernel function in Equ. (4) in the AFF emulator, to capture permutational symmetries between PE atoms. Conditional on γ and λ , the maximum likelihood estimator (MLE) of σ_i^2 is $\hat{\sigma}_i^2 = S_i^2/M$ with $S_i^2 = \mathbf{F}_i^T(\mathbf{R} + \lambda\mathbf{I}_{3Ml_i})^{-1}\mathbf{F}_i$ for the i th PE atom set. The nugget parameter λ and the range parameter γ can be estimated through MLE through numerically optimizing the profile likelihood or through the cross validation with respect to squared error loss in predictions. When the number of training configurations is small, the marginal posterior mode may be used to avoid unstable estimation of the range and nugget parameters³⁵.

Conditional on the estimated parameters $\hat{\theta}_i = [\hat{\sigma}_i^2, \hat{\gamma}, \hat{\lambda}]$, the predictive distribution of forces of atoms in the i th PE atom set $\mathbf{F}_i(\mathbf{D}(\mathbf{x}^*))$ at any atoms' positions \mathbf{x}^* follows a multivariate normal distribution

$$(\mathbf{F}_i(\mathbf{D}(\mathbf{x}^*)) | \mathbf{F}_i, \hat{\theta}_i) \sim \mathcal{MN}(\hat{\mathbf{F}}_i(\mathbf{D}(\mathbf{x}^*)), \hat{\sigma}_i^2 \mathbf{K}^*(\mathbf{x}^*, \mathbf{x}^*)), \quad (8)$$

where the predictive mean vector and predictive covariance matrix follows

$$\hat{\mathbf{F}}_i(\mathbf{D}(\mathbf{x}^*)) = \mathbf{R}_{\mathbf{x}^*}^T(\mathbf{R} + \hat{\lambda}\mathbf{I}_{3Ml_i})^{-1}\mathbf{F}_i, \quad (9)$$

$$\hat{\sigma}_i^2 \mathbf{K}^*(\mathbf{x}^*, \mathbf{x}^*) = \hat{\sigma}_i^2(\mathbf{R}^* - \mathbf{R}_{\mathbf{x}^*}^T(\mathbf{R} + \hat{\lambda}\mathbf{I}_{3Ml_i})^{-1}\mathbf{R}_{\mathbf{x}^*}), \quad (10)$$

with \mathbf{R}^* being a $3l_i \times 3l_i$ Hessian matrix of the kernel function $\nabla_{\mathbf{x}^*i} K(\mathbf{D}(\mathbf{x}^*), \mathbf{D}(\mathbf{x}^*)) \nabla_{\mathbf{x}^*i}^T$. Note that the pre-

dictive mean in Equ. (9) is exactly the same as KRR estimator in Equ. (5). The advantage herein is the quantified uncertainty of predictions, as the predictive distribution follows a multivariate normal distribution. The uncertainty assessment of predictions is important to determine a sequential design for efficiently emulating computationally expensive simulations.

Note that the computational cost of the AFF model is much smaller than that of GDML, sGDML, or a joint model using both force and energy^{9,10,13}, as the covariance matrix of the AFF model is $3Ml_i \times 3Ml_i$ for the i th PE atom set, which is much smaller than the $3MN \times 3MN$ covariance matrix in the GDML or sGDML model. Computing the likelihood function and predictive mean of the AFF model only costs $\mathcal{O}(NM^3)$ for M training configurations of a molecule with N PE atoms, whereas the computational cost of predictive mean from GDML or sGDML is $\mathcal{O}((NM)^3)$ in comparison.

C. Predicting potential energy through the AFF model

Emulating energy based on simulated force vector and energy could also induce high computational costs, due to computation of inversion of large covariance matrix of simulated force vector and energy¹³. Here we introduce a computationally feasible approach to emulate the potential energy. For any molecule with atomic configuration \mathbf{x}^* , the potential energy $E(\mathbf{x}^*)$ correlates with the vector of potential energy from previously simulated molecular configurations $\mathbf{E} = (E(\mathbf{x}_1), \dots, E(\mathbf{x}_M))$, and the atomic force at this molecular configuration $\mathbf{F}(\mathbf{x}^*)$ (noting that $\mathbf{F}(\mathbf{x}^*)$ is not observed). Conditional on \mathbf{E} and $\mathbf{F}(\mathbf{x}^*)$, the correlation between $E(\mathbf{x}^*)$ and forces at other configurations is small. Thus the predictive distribution of $E(\mathbf{x}^*)$ conditional on both simulated energy and atomic force ($E(\mathbf{x}^*) | \mathbf{E}, \mathbf{F}$) can be approximated by ($E(\mathbf{x}^*) | \mathbf{E}, \mathbf{F}(\mathbf{x}^*)$), where $\mathbf{F}(\mathbf{x}^*)$ can be estimated by the predictive distribution in the AFF model discussed in Section II B. The motivation of method is relevant to the induced point approximation approach of Gaussian processes^{7,15}, where given outcomes of a function at a set of well-chosen induced pseudo-inputs, the predictive distribution of the outcome at a new input is assumed to be conditionally independent to outputs in the training dataset. Here the induced input points of $E(\mathbf{x}^*)$ are $(\mathbf{E}, \mathbf{F}(\mathbf{x}^*))$, due to large correlation between these variables. Conditional on $(\mathbf{E}, \mathbf{F}(\mathbf{x}^*))$, we assume the force vector $\mathbf{F}(\mathbf{x}^*)$ at this configuration is approximately independent to other training configurations of force vectors. This simplification avoids constructing and computing the large Hessian covariance matrix of force vectors, allowing us to perform inversion of a $(3N + M) \times (3N + M)$ covariance matrix, instead of inversion of a $(3N + 1)M \times (3N + 1)M$ covariance matrix, in computing the predictive distribution of energy at this configuration. When we need to predict energy at many new molecular settings, matrix inversion of the sub-

covariance matrix for simulated energy is shared among all predictive distributions. Thus they are only needed to be computed once. Details of efficient computation for predictive distributions of energy, and model extension by conditioning on a small batch of force vectors (instead of only one force vector) to improve predictive accuracy, are discussed in Appendix B.

For any molecule with atomic coordinates \mathbf{x}^* , denote a combined vector of force and energy $\mathbf{EF} = (E(\mathbf{x}^*), \mathbf{E}^T, \mathbf{F}^T(\mathbf{x}^*))^T$, where $E(\mathbf{x}^*)$ is the potential energy of molecule with atomic coordinates being \mathbf{x}^* , and $\mathbf{F}(\mathbf{x}^*)$ is the force field vector of this molecule. Assuming a GP model for potential energy with covariance function $K(\cdot, \cdot)$ and mean function $\mu(\cdot)$, the random vector \mathbf{EF} follows a multivariate normal distribution:

$$\mathbf{EF} \sim \mathcal{MN}(\boldsymbol{\mu}_{EF}, \boldsymbol{\Sigma}_{EF}), \quad (11)$$

where the mean vector follows

$$\boldsymbol{\mu}_{EF} = (\mu(\mathbf{x}^*), \boldsymbol{\mu}_{\mathbf{X}}^T, -\nabla_{\mathbf{r}}\mu(\mathbf{x}^*)^T)^T,$$

with $\mu(\mathbf{x}^*)$ assumed to be an unknown constant m (estimated by MLE in this work), and $\boldsymbol{\mu}_{\mathbf{X}} = m\mathbf{1}_M$. The covariance matrix in Equ. (11) follows

$$\boldsymbol{\Sigma}_{EF} = \sigma^2 \left(\begin{bmatrix} K_{\mathbf{x}^*, \mathbf{x}^*} & \mathbf{K}_{\mathbf{X}, \mathbf{x}^*} & -\mathbf{J}_{\mathbf{x}^*, \mathbf{x}^*}^T \\ \mathbf{K}_{\mathbf{x}^*, \mathbf{X}} & \mathbf{K}_{\mathbf{X}, \mathbf{X}} & -\mathbf{J}_{\mathbf{X}, \mathbf{x}^*}^T \\ -\mathbf{J}_{\mathbf{x}^*, \mathbf{x}^*} & -\mathbf{J}_{\mathbf{x}^*, \mathbf{X}} & \mathbf{R}_{\mathbf{x}^*, \mathbf{x}^*} \end{bmatrix} + \lambda \mathbf{I}_{M+3N+1} \right),$$

where the upper left 4 matrix blocks are the covariance of energy vectors $(E(\mathbf{x}^*), \mathbf{E}^T)^T$. The (i, j) element of the correlation matrix $K_{\mathbf{X}, \mathbf{X}}$ is $K(\mathbf{D}(\mathbf{x}_i), \mathbf{D}(\mathbf{x}_j))$, for $i = 1, \dots, M$ and $j = 1, \dots, M$, and $K_{\mathbf{x}^*, \mathbf{x}^*} = 1$ (denoting the correlation of total energy between the configuration \mathbf{x}^* and itself). The vector $\mathbf{K}_{\mathbf{x}^*, \mathbf{X}} = \mathbf{K}_{\mathbf{X}, \mathbf{x}^*}^T = (K(\mathbf{D}(\mathbf{x}^*), \mathbf{D}(\mathbf{x}_1)), \dots, K(\mathbf{D}(\mathbf{x}^*), \mathbf{D}(\mathbf{x}_M)))^T$ denotes the correlation between the potential energy at input \mathbf{x}^* and the potential energy at training inputs \mathbf{X} . Besides, the $3N \times 3N$ correlation matrix between forces is denoted by $\mathbf{R}(\mathbf{x}^*, \mathbf{x}^*) = \nabla_{\mathbf{x}^*} K(\mathbf{D}(\mathbf{x}^*), \mathbf{D}(\mathbf{x}^*)) \nabla_{\mathbf{x}^*}^T$. Finally, \mathbf{J} denotes the correlation between energy and forces. Here $\mathbf{J}_{\mathbf{x}^*, \mathbf{X}}$ is a $3N \times M$ matrix with the j th column being $\nabla_{\mathbf{x}^*} K(\mathbf{D}(\mathbf{x}^*), \mathbf{D}(\mathbf{x}_j))$ for $j = 1, 2, \dots, M$, and $\mathbf{J}_{\mathbf{x}^*, \mathbf{x}^*}$ is the correlation matrix between force and energy for molecule configuration with atom positions \mathbf{x}^* .

Similar to parameter estimation of AFF model discussed in Sec. II B, the mean and variance parameter can be estimated by the MLE of the simulated (training) energy vector below

$$\hat{m} = (\mathbf{1}_M^T (\mathbf{K}_{\mathbf{X}, \mathbf{X}} + \lambda \mathbf{I}_M)^{-1} \mathbf{1}_M)^{-1} \mathbf{1}_M^T (\mathbf{K}_{\mathbf{X}, \mathbf{X}} + \lambda \mathbf{I}_M)^{-1} \mathbf{E}$$

$$\hat{\sigma}^2 = \frac{(\mathbf{E} - \mathbf{1}\hat{m})^T (\mathbf{K}_{\mathbf{X}, \mathbf{X}} + \lambda \mathbf{I}_M)^{-1} (\mathbf{E} - \mathbf{1}\hat{m})}{M}.$$

The range parameter γ and the nugget parameter λ in the kernel function can be estimated through numerical optimization by cross-validation or MLE.

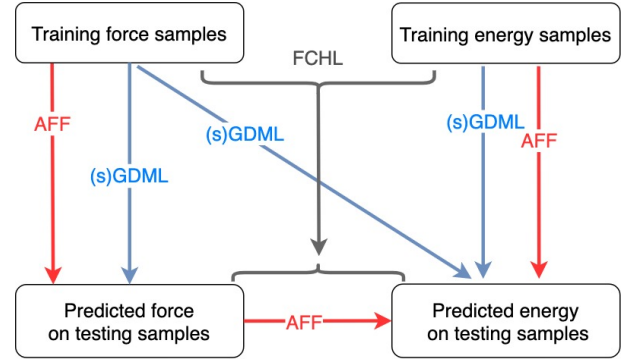


FIG. 2. Schematic representation of different approaches in predicting atomic force and potential energy of molecules. GDML and sGDML methods predict force of molecule at a new configuration based on forces on simulated configurations. The predictive force and energy were used to estimate the energy of this molecule. The FCHL method estimates the energy and atomic force by a joint model fitted using both the simulated force and energy samples. The AFF method partitions the atoms into PE atoms set and the atomic force of atoms of a new configuration is predicted based on the simulated force of atoms in the same PE set. The energy of molecule at this configuration was predicted based on the predicted atomic force and energy from simulated samples.

Based on previous discussion, assuming that the given $(\mathbf{E}, \mathbf{F}(\mathbf{x}^*))$, $E(\mathbf{x}^*)$ is approximately independent of the rest of force vectors, then we have

$$(E(\mathbf{x}^*) | \mathbf{E}, \mathbf{F}, \hat{m}, \hat{\sigma}^2, \hat{\gamma}, \hat{\lambda}) \sim \mathcal{MN}(\hat{E}(\mathbf{x}^*), \hat{\sigma}^2 K_E^*(\mathbf{x}^*, \mathbf{x}^*)), \quad (12)$$

where \sim denotes the approximation of the predictive distribution, and the predictive mean is a weighted average of training energy \mathbf{E} and training force \mathbf{F} :

$$\hat{E}(\mathbf{x}^*) = \omega_E^* \mathbf{E} + \omega_F^* \mathbf{F}. \quad (13)$$

Closed form expressions of ω_E^* , ω_F^* and $\mathbf{K}_E^*(\mathbf{x}^*, \mathbf{x}^*)$ are derived in Appendix C.

In practice, the noise term is added to the distribution of \mathbf{EF} from Equ. (11), and the energy on the testing set is estimated in batches using the conditional distribution at Equ. (12). A particular benefit of our method is that we exploit the estimable information from the force but avoid computing the inverse of the gigantic kernel matrix on \mathbf{F} , which substantially simplifies the computation.

The comparison between our predictive model and GDML model for predicting the energy is illustrated in Fig. 2. For GDML, as well as for both sGDML and FCHL, all simulated energy and force are used, but inversion of a large covariance matrix is computationally expensive. Here, conditional on the simulated energy and force of a new molecular configuration, we assume the potential energy of a new molecule is independent of forces of other molecular configuration simulated before. Since our approach does not need to handle the $3N \times 3N$ covariance matrix of the force, our method is

scalable to large molecules and potentially emulating MD simulations with multiple molecules.

III. NUMERICAL RESULTS

We evaluate the performance of the AFF approach by analyzing the required training time and learning curves on a variety of molecules, including benzene, uracil, and naphthalene from the MD17 dataset, and aspirin, alpha-glucose, hexadecane from our simulated dataset. We compare the predictive error and required training time from AFF with some of the most commonly used KRR-based models, such as the GDML and sGDML approaches for force and energy predictions. All comparisons are implemented under the same training and testing set. In addition, we also provide the uncertainty assessment of the predictions from our model through the number of held-out outcomes covered in the 95% predictive interval, the average length of the predictive interval (see Table. I for details on the prediction accuracy, required training time, and uncertainty assessment of the AFF predictions), the ratio of the average length of the predictive interval to the range of testing forces L^{norm} , and the difference between 95% confidence level and the proportion of the held-out samples contained in the predictive interval $\Delta p_{CI}^{0.95}$ on held-out dataset (see Fig 5 for the detail of L^{norm} and $\Delta p_{CI}^{0.95}$ on those six molecules). An efficient method should have small mean squared error, small training cost, short average length of the predictive interval, and around 95% of the held-out test data covered by the 95% predictive interval. Furthermore, the comparison between our method with sparse approximation method in a SOAP model^{1,7} is given in the supplementary material. We do not include them in this section as our method seems to be an order of magnitude more accurate than the method with a sparse approximation to the covariance matrix, in terms of out of sample predictions.

Previous studies have shown that the GDML and sGDML have relatively small error, compared with other approaches^{10,13}. Indeed according to Fig. 3, the error of both approaches is relatively small. However, both GDML and sGDML has a large computational cost, mainly due to the inversion of $3NM \times 3NM$ covariance matrix of force vectors at all training configurations. Because of the reduced computational order on force prediction by partitioning the atoms into PE atom sets, the AFF model has smaller predictive error of force prediction (blue curves) when using similar or even less training time (blue histograms) compared to GDML and sGDML approaches. The improved accuracy of force predictions by the AFF model is even more noticeable on the additional simulation of aspirin, alpha-glucose and hexadecane shown in Fig. 3.

The sGDML approach typically has a smaller error compared with GDML when there are at least two PE atom sets exist in simulation, such as the simulation

of benzene, aspirin and naphthalene molecule, consistent with the result reported in literature¹⁰. This is because the PS kernel in Equ. (4) allows the sGDML approach to properly represent the large correlation of forces between atoms in the PE atom set. Note that here the reduced computational complexity in AFF allows us to train our models with more observations than the GDML and sGDML approaches for predicting the force with a even smaller computational budget. The number of training observations required in training the AFF model, however, is still very small (from a few hundred to a thousand). This differs from some recent studies of deep neural network approaches^{11,12,36,37}, where a much larger set of training observations (ranging from 10^4 to 10^5) are required. The computational cost of obtaining a substantially larger simulation data set by deep neural network approaches is not negligible.

Given the same number of observations, the error in predicting the potential energy by the AFF model is typically smaller than the sGDML and GDML approaches, shown in the second rows of Fig. 3. For some of test molecules, such as naphthalene and benzene in the MD17 data set, and aspirin and alpha-glucose in our simulated data set, the AFF model has much smaller predictive error than sGDML approach. This is because our approach incorporates both force and energy vectors in energy prediction through a joint statistical model, and making predictions on energy based on both simulated force and energy vectors. The joint model of force and energy was recently studied in¹³, whereas directly implementing the conditional prediction incurs large computational cost. Here the approximation by the induced point approach introduced in Sec. IIC allows us to keep the computational complexity of predicting the energy the same as predicting the force, whereas maintaining high predictive accuracy as that in¹³. For larger molecules, like alpha-glucose, aspirin, and hexadecane (with 21 to 51 atoms) in our simulated dataset, the computation reduction is huge (see the blue histograms in Fig. 3). For these examples, AFF achieves higher accuracy in predicting atomic force, despite costing less than 10% of the training time of the sGDML approach, as shown in Table. I. Therefore, our approach is potentially applicable to emulate the physical quantities of interest for simulation of larger molecules containing many more atoms.

Among all molecules we compared, the AFF model has a larger predictive error for the uracil, using the same number of training input (third panel in the second row in Fig. 3). Since the AFF model estimates the energy based on the emulated atomic force, the accuracy of energy prediction would be reduced when the emulated force is not accurate. As shown in the Fig. 3, the estimated force by AFF for uracil is not accurate when the number of training sample is small. This problem can be solved by using a moderately large sample size (≈ 1000) to achieve similarly accurate predictions as the sGDML model. The predictive energy vector by the AFF model along the AIMD trajectories is graphed in Figure 4 along with the

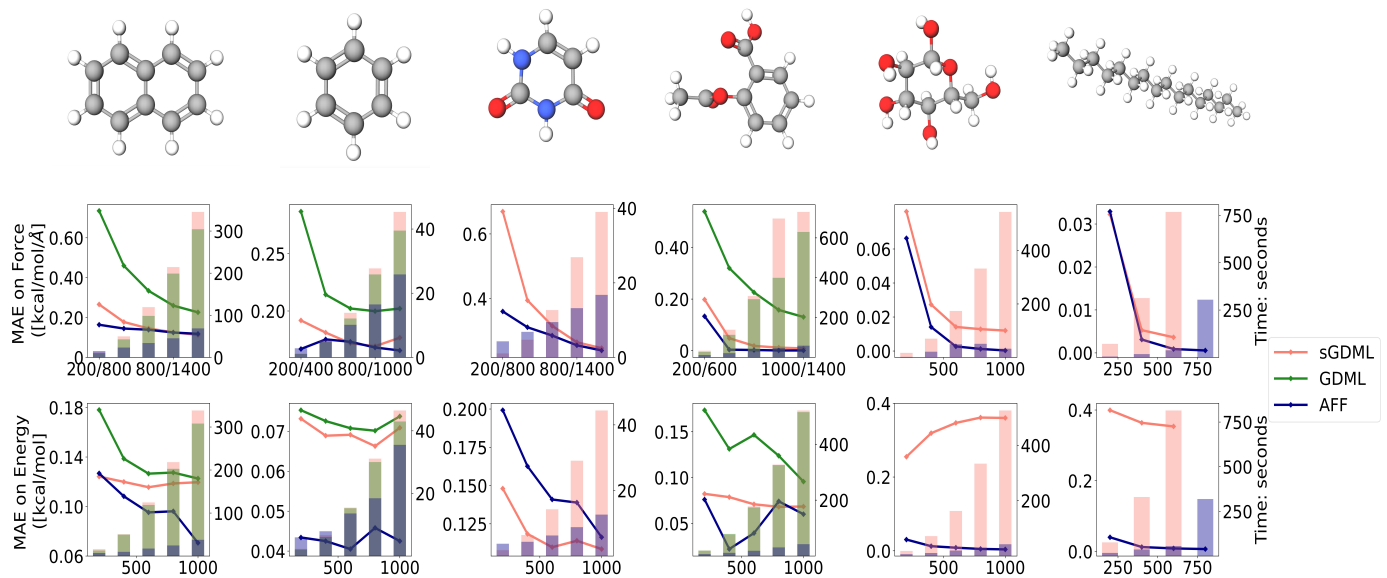


FIG. 3. The learning curves for force and energy on naphthalene, benzene, uracil from the MD17 dataset, and aspirin, alpha-glucose, hexadecane from our simulated dataset (ordered from left to right). Learning curves are presented for the GDML and sGDML methods as well as the AFF method under the same training, validation and testing set. The training sample size (x-axis) are twofold for AFF method on force prediction. The AFF uses a larger training set for predicting forces for the first 4 molecules, and the computational time (shown as the blue bars) is still much lower compared with the GDML and sGDML approaches. The top row contains the learning curve (in terms of mean absolute error (MAE)) and training time for the out-of-sample force prediction. The bottom row contains the learning curve and training time for the out-of-sample energy prediction. GDML and sGDML approach are equivalent on uracil, alpha-glucose and hexadecane, as all atoms are permutationally distinct. Thus only two learning curves are shown for those molecules.

held-out energy in the simulation. Also plotted are the predictive atomic forces and the truth at two held-out configurations. Based on $M = 800$ simulated forces and energies, predictions of potential energies and forces by the AFF model are accurate.

Table. I gives the predictive error of force vectors and energy, the percentage of forces covered in the predictive interval, the average length of the predictive intervals of forces and computational costs in emulation from different methods. Firstly, the predictive error of AFF methods for both forces and energy is typically not larger than the sGDML approach. For some molecules such as alpha-glucose and hexadecane, the predictive error of the AFF model seems to be one order of magnitude smaller, based on the same held-out test set. It is worth noting that it takes the AFF model much smaller computational costs (ranging from 1/2 to 1/30 of costs compared to sGDML) to achieve the higher level of predictive accuracy. These results indicate the AFF model is more efficient in emulating atomic forces and energy in AIMD simulation. Moreover, around 95% (or higher percentage) of the held-out atomic forces are covered by relatively short 95% predictive intervals from the AFF approach, indicating that AFF model provides a reliable way to quantify the uncertainty in predictions.

Furthermore, it is worth mentioning that the reduction of computational cost by the AFF model is more pronounced on molecules with more PE atoms' sets, such as alpha-glucose, aspirin, and hexadecane. For molecules with fewer PE sets such as benzene (where we can only partition the atoms into two PE sets for each configurations), the computational reduction will be smaller. Thus, our approach may be useful for reducing the computational cost of interactions between a large number of molecules, as most PE sets may only contain one atom.

Finally, uncertainty assessments of predictions of the AFF approach are given in Fig. 5. Compared with the range of observations, the average length of 95% (pink bar) is much shorter, indicating small uncertainty associated with predictions. The difference between the number of held-out test samples covered 95% interval and the nominal 95% range (blue curves) is small, meaning that the uncertainty is accurately quantified. The internal assessment of the uncertainty of the AFF model can be used to identify the input region with large uncertainty, and sequentially design simulation runs for uncertainty reduction or Bayesian optimization^{23,38}.

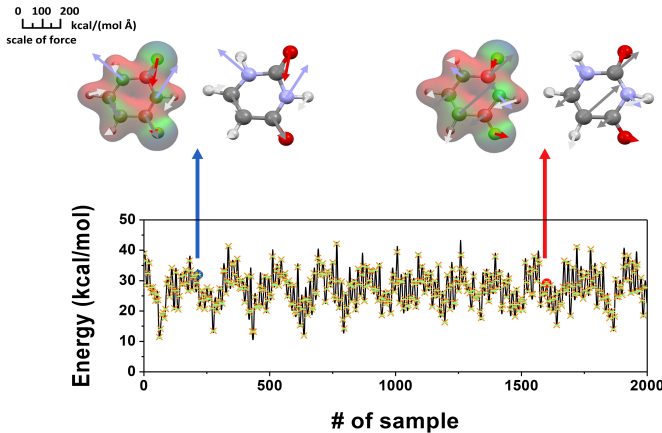


FIG. 4. Energy of uracil obtained from the AFF method along the AIMD trajectories, where the AIMD energies are displayed in black curve and predictions of held-out energies from the AFF model are graphed in yellow crosses. The green bars are the 95% predictive intervals of the AFF energies. As the length of the intervals is very small, the intervals almost overlap with the AIMD energies and they are nearly invisible. Depicted above the panel of energy in the upper half of the figure is a comparison of AIMD atomic forces and predicted atomic forces by the AFF model on two randomly selected molecules. Within each of the two pairs shown, the same molecule is illustrated twice with the depiction on the left displaying AIMD atomic forces and the depiction on the right displaying the atomic forces by the AFF model. $M = 800$ simulated forces and energies were used to train the AFF model for predictions.

IV. CONCLUDING REMARKS

We have proposed an accurate and computationally efficient approach to predict potential energy surfaces and molecular force fields in *ab initio* simulation. While the theoretical framework of the gradient-based KRR and GP models such as GDML, sGDML, and FCHL, were already established, the challenge posed by the huge computational cost limited the applicability of these methods in emulating systems with a larger size of molecules. We propose the AFF emulator to overcome this computational challenge without compromising its accuracy. The efficient emulation of forces was hinged upon the fact that the similarity of atomic forces between permutationally equivalent atoms is high, whereas the correlation is small across different permutationally equivalent atom sets. By partitioning the atoms of a molecule into different atom sets, the AFF model can capture large correlation of forces between PE atoms, thereby providing accurate predictions of atomic forces of the molecule at a new configuration with less computational costs. Second, we introduced the induced input approach to reduce the computational complexity for emulating the potential energy, compared to the joint model of energy and atomic forces of simulated configurations. Numerical results have shown predictions are more accurate than some al-

Molecule	Energy [kcal/mol]	Force [kcal/mol/Å]	Training Time [s]	P_{CI} (95%)	L_{CI} (95%)
Naphthalene	0.07 (0.12)	0.11 (0.11)	68 (345)	98.5%	1.36
Benzene	0.04 (0.07)	0.173 (0.176)	23 (45)	85%	0.7
Uracil	0.10 (0.10)	0.239 (0.249)	16 (43)	97.8%	2.37
Alpha-glucose	0.09 (0.36)	0.0003 (0.012)	32 (964)	100%	0.03
Hexadecane	0.008 (0.35)	0.0008 (0.003)	37 (767)	99%	0.05
Aspirin	0.06 (0.09)	0.0028 (0.009)	32 (629)	99.8%	0.08

TABLE I. The second and third column show the MAE on estimated energy and force. The fourth column is the training time of the model at shown force accuracy, which is provided in seconds. The numbers in parentheses are the sGDML results, and they are tested under same held-out test set. The specific criteria employed are the following: $P_{CI}(95\%) = \frac{1}{3NM^*} \sum_{i=1}^{M^*} \sum_{j=1}^{3N} 1\{\mathbf{F}(\mathbf{x}_i^*)_j\} \in CI_{ij}(95\%)$, $L_{CI}(95\%) = \frac{1}{3NM^*} \sum_{i=1}^{M^*} \sum_{j=1}^{3N} length\{CI_{ij}(95\%)\}$, where M^* is the number of test samples, $\mathbf{F}(\mathbf{x}_i^*)_j$ is the j_{th} element from the force vector prediction of the output of the i_{th} held-out molecule; $CI_{ij}(95\%)$ is the 95% predictive credible interval from the multivariate normal distribution in (8); and $length\{CI_{ij}(95\%)\}$ is the length of the 95% predictive credible interval. The number of training samples used in AFF and sGDML (in parentheses) method is: naphthalene 1600 (1000), benzene 1200 (1000), uracil 1600 (1000), alpha-glucose 1000 (1000), aspirin 1200 (1000), and hexadecane 600 (600).

ternative approaches, given the same computational budget. The AFF approach discovers a novel path on representing correlation between forces and energy with significantly lower computational cost. We anticipate that our approach will enable chemists to run fast and accurate molecular dynamics simulations on larger molecules with machine learned potentials and forces throughout chemical space.

There are a few potential research directions of emulating simulations of a large-scale system with interactions between a large number of atoms. First, for emulating simulation involving a large number of molecules, one may represent interactions between atoms by partitioning the atoms into PE atoms to decompose the covariance matrix for efficient computation. Second, sparse Cholesky factorization or Markov models may be used to reduce the large computational cost when the required number of simulations used in training machine learning models gets large. Third, given a set of physical constraints, one may inversely design the atomic positions to achieve a particular force field, or potential energy. The uncertainty of the map from atomic positions to potential energy learned by the AFF model is important for a sequential design to reduce the uncertainty of this problem. These improvements can empower the molecular dynamics simulation for large molecules with the cost of cMD and accuracy of AIMD.

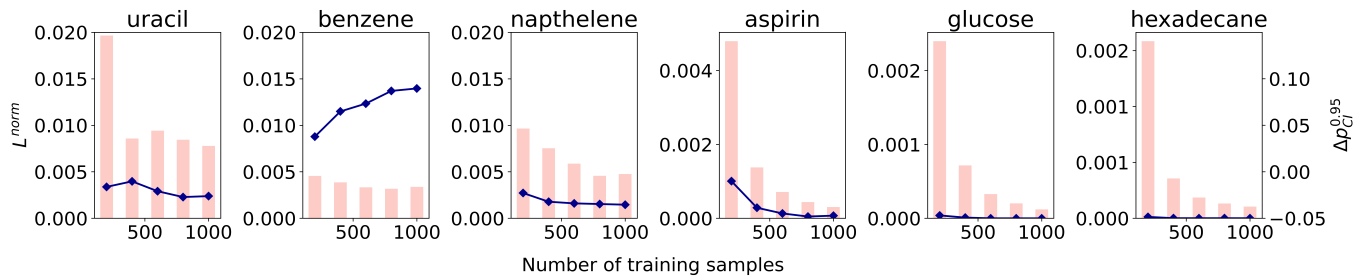


FIG. 5. The bar charts show the proportion of average AFF predicted atomic force confidence interval $L_{CI}(95\%)$ over the range from testing samples changing with the number of training samples. The blue line charts show the difference Δp between confidence level 0.95 and actual coverage of AFF predicted atomic force confidence level. The proportion L^{norm} is given by $\rho = L_{CI}(95\%)/\text{range}(\mathbf{F}(\mathbf{x}^*))$, where $L_{CI}(95\%) = \frac{1}{3NM^*} \sum_{i=1}^{M^*} \sum_{j=1}^{3N} \text{length}\{CI_{ij}(95\%)\}$, and $\text{range}(\mathbf{F}(\mathbf{x}^*)) = \max(\mathbf{F}(\mathbf{x}^*)) - \min(\mathbf{F}(\mathbf{x}^*))$. The $\Delta p_{CI}^{0.95}$ is given by $\Delta p_{CI}^{0.95} = 0.95 - P_{CI}(95\%)$, where $P_{CI}(95\%) = \frac{1}{3NM^*} \sum_{i=1}^{M^*} \sum_{j=1}^{3N} 1\{\mathbf{F}(\mathbf{x}_i^*)_j\} \in CI_{ij}(95\%)$.

ACKNOWLEDGEMENTS

This study was supported by the U.S. National Science Foundation’s Computational and Data-Enabled Science and Engineering program under Award No. 2053423. MZ and JW acknowledge financial support from the U.S. National Science Foundation’s Harnessing the Data Revolution (HDR) Big Ideas Program under Grant no. NSF 1940118.

DATA AVAILABILITY

The data that support the findings of this study are available from the corresponding author upon reasonable request.

- ¹A. P. Bartók, R. Kondor, and G. Csányi, “On representing chemical environments,” *Physical Review B* **87**, 184115 (2013).
- ²A. P. Bartók, J. Kermode, N. Bernstein, and G. Csányi, “Machine learning a general-purpose interatomic potential for silicon,” *Physical Review X* **8**, 041048 (2018).
- ³D. Lu, H. Wang, M. Chen, L. Lin, R. Car, E. Weinan, W. Jia, and L. Zhang, “86 pflops deep potential molecular dynamics simulation of 100 million atoms with ab initio accuracy,” *Computer Physics Communications* **259**, 107624 (2021).
- ⁴M. Rupp, A. Tkatchenko, K.-R. Müller, and O. A. Von Lilienfeld, “Fast and accurate modeling of molecular atomization energies with machine learning,” *Physical review letters* **108**, 058301 (2012).
- ⁵J. Wu and M. Gu, “Emulating the first principles of matter: A probabilistic roadmap,” *arXiv preprint arXiv:2010.05942* (2020).
- ⁶A. P. Bartók and G. Csányi, “Gaussian approximation potentials: A brief tutorial introduction,” *International Journal of Quantum Chemistry* **115**, 1051–1057 (2015).
- ⁷E. Snelson and Z. Ghahramani, “Sparse Gaussian processes using pseudo-inputs,” *Advances in neural information processing systems* **18**, 1257 (2006).
- ⁸J. Gilmer, S. S. Schoenholz, P. F. Riley, O. Vinyals, and G. E. Dahl, “Neural message passing for quantum chemistry,” in *International conference on machine learning* (PMLR, 2017) pp. 1263–1272.
- ⁹S. Chmiela, A. Tkatchenko, H. E. Sauceda, I. Poltavsky, K. T. Schütt, and K.-R. Müller, “Machine learning of accurate energy-conserving molecular force fields,” *Science advances* **3**, e1603015 (2017).

- ¹⁰S. Chmiela, H. E. Sauceda, K.-R. Müller, and A. Tkatchenko, “Towards exact molecular dynamics simulations with machine-learned force fields,” *Nature communications* **9**, 1–10 (2018).
- ¹¹K. T. Schütt, H. E. Sauceda, P.-J. Kindermans, A. Tkatchenko, and K.-R. Müller, “Schnet—a deep learning architecture for molecules and materials,” *The Journal of Chemical Physics* **148**, 241722 (2018).
- ¹²L. Zhang, J. Han, H. Wang, R. Car, and E. Weinan, “Deep potential molecular dynamics: a scalable model with the accuracy of quantum mechanics,” *Physical review letters* **120**, 143001 (2018).
- ¹³A. S. Christensen, L. A. Bratholm, F. A. Faber, and O. Anatole von Lilienfeld, “FCHL revisited: Faster and more accurate quantum machine learning,” *The Journal of Chemical Physics* **152**, 044107 (2020).
- ¹⁴S. Chmiela, H. E. Sauceda, I. Poltavsky, K.-R. Müller, and A. Tkatchenko, “sGDML: Constructing accurate and data efficient molecular force fields using machine learning,” *Computer Physics Communications* **240**, 38–45 (2019).
- ¹⁵A. Wilson and H. Nickisch, “Kernel interpolation for scalable structured Gaussian processes (KISS-GP),” in *International Conference on Machine Learning* (PMLR, 2015) pp. 1775–1784.
- ¹⁶N. Cressie and G. Johannesson, “Fixed rank kriging for very large spatial data sets,” *Journal of the Royal Statistical Society: Series B (Statistical Methodology)* **70**, 209–226 (2008).
- ¹⁷C. G. Kaufman, M. J. Schervish, and D. W. Nychka, “Covariance tapering for likelihood-based estimation in large spatial data sets,” *Journal of the American Statistical Association* **103**, 1545–1555 (2008).
- ¹⁸A. Datta, S. Banerjee, A. O. Finley, and A. E. Gelfand, “Hierarchical nearest-neighbor gaussian process models for large geostatistical datasets,” *Journal of the American Statistical Association* **111**, 800–812 (2016).
- ¹⁹F. Lindgren, H. Rue, and J. Lindström, “An explicit link between gaussian fields and gaussian markov random fields: the stochastic partial differential equation approach,” *Journal of the Royal Statistical Society: Series B (Statistical Methodology)* **73**, 423–498 (2011).
- ²⁰H. Rue, S. Martino, and N. Chopin, “Approximate bayesian inference for latent gaussian models by using integrated nested laplace approximations,” *Journal of the royal statistical society: Series B (statistical methodology)* **71**, 319–392 (2009).
- ²¹R. B. Gramacy and D. W. Apley, “Local Gaussian process approximation for large computer experiments,” *Journal of Computational and Graphical Statistics* **24**, 561–578 (2015).
- ²²J. R. Stroud, M. L. Stein, and S. Lysen, “Bayesian and maximum likelihood estimation for gaussian processes on an incomplete lattice,” *Journal of computational and Graphical Statistics* **26**, 108–120 (2017).

- ²³B. Shahriari, K. Swersky, Z. Wang, R. P. Adams, and N. De Freitas, "Taking the human out of the loop: A review of bayesian optimization," *Proceedings of the IEEE* **104**, 148–175 (2015).
- ²⁴F. de Roos, A. Gessner, and P. Hennig, "High-dimensional gaussian process inference with derivatives," *arXiv preprint arXiv:2102.07542* (2021).
- ²⁵D. Eriksson, K. Dong, E. H. Lee, D. Bindel, and A. G. Wilson, "Scaling gaussian process regression with derivatives," *arXiv preprint arXiv:1810.12283* (2018).
- ²⁶Z. Xie and J. M. Bowman, "Permutationally invariant polynomial basis for molecular energy surface fitting via monomial symmetrization," *Journal of Chemical Theory and Computation* **6**, 26–34 (2010).
- ²⁷B. Jiang and H. Guo, "Permutation invariant polynomial neural network approach to fitting potential energy surfaces. iii. molecule-surface interactions," *The Journal of Chemical Physics* **141**, 034109 (2014).
- ²⁸D. Koner and M. Meuwly, "Permutationally invariant, reproducing kernel-based potential energy surfaces for polyatomic molecules: From formaldehyde to acetone," *Journal of Chemical Theory and Computation* **16**, 5474–5484 (2020).
- ²⁹S. Uneyama, "An eigendecomposition approach to weighted graph matching problems," *IEEE transactions on pattern analysis and machine intelligence* **10**, 695–703 (1988).
- ³⁰C. E. Rasmussen, *Gaussian processes for machine learning* (MIT Press, 2006).
- ³¹M. Kanagawa, P. Hennig, D. Sejdinovic, and B. K. Sriperumbudur, "Gaussian processes and kernel methods: A review on connections and equivalences," *arXiv preprint arXiv:1807.02582* (2018).
- ³²M. Gu and J. O. Berger, "Parallel partial Gaussian process emulation for computer models with massive output," *Annals of Applied Statistics* **10**, 1317–1347 (2016).
- ³³O. Roustant, D. Ginsbourger, and Y. Deville, "Dicekriging, diceoptim: Two R packages for the analysis of computer experiments by kriging-based metamodeling and optimization," (2012).
- ³⁴M. Gu, J. Palomo, and J. O. Berger, "RobustGaSP: Robust Gaussian Stochastic Process Emulation in R," *The R Journal* **11**, 112–136 (2019).
- ³⁵M. Gu, "Jointly robust prior for Gaussian stochastic process in emulation, calibration and variable selection," *Bayesian Analysis* **14** (2018).
- ³⁶Y. Zhang, C. Hu, and B. Jiang, "Embedded atom neural network potentials: Efficient and accurate machine learning with a physically inspired representation," *The journal of physical chemistry letters* **10**, 4962–4967 (2019).
- ³⁷O. T. Unke and M. Meuwly, "Physnet: a neural network for predicting energies, forces, dipole moments, and partial charges," *Journal of chemical theory and computation* **15**, 3678–3693 (2019).
- ³⁸J. Snoek, H. Larochelle, and R. P. Adams, "Practical bayesian optimization of machine learning algorithms," *Advances in neural information processing systems* **25** (2012).

Appendix A: The correlation of force between different atoms

The correlation between the force of two molecules a and b with positions \mathbf{x}_a and \mathbf{x}_b is a $3N \times 3N$ matrix $\mathbf{R}(\mathbf{x}_a, \mathbf{x}_b)$, where the (i, j) element follows $(\mathbf{R}(\mathbf{x}_a, \mathbf{x}_b))_{ij} = \nabla_{\mathbf{r}^{ai}} K(\mathbf{D}(\mathbf{x}_a), \mathbf{D}(\mathbf{x}_b)) \nabla_{\mathbf{r}^{bj}}^T$. Direct computation through the chain rule gives $\nabla_{\mathbf{r}^{ai}} K(\mathbf{D}(\mathbf{x}_a), \mathbf{D}(\mathbf{x}_b)) = \sum_{p,q=1}^N \frac{\partial \mathbf{D}(\mathbf{x}_a)_{pq}}{\partial \mathbf{r}^{ai}} \frac{\partial K(\mathbf{D}(\mathbf{x}_a), \mathbf{D}(\mathbf{x}_b))}{\partial \mathbf{D}(\mathbf{x}_a)_{pq}}$. Based on the form of the descriptor matrix $\mathbf{D}(\mathbf{x})$ in Equ.

(2), the gradient of (p, q) element of $\mathbf{D}(\mathbf{x})$ w.r.t \mathbf{r}_i follows

$$\frac{\partial \mathbf{D}(\mathbf{x})_{pq}}{\partial \mathbf{r}_i} = \begin{cases} -\frac{\mathbf{r}_p - \mathbf{r}_q}{\|\mathbf{r}_p - \mathbf{r}_q\|^3} & p > q \text{ and } i = p, \\ \frac{\mathbf{r}_p - \mathbf{r}_q}{\|\mathbf{r}_p - \mathbf{r}_q\|^3} & p > q \text{ and } i = q, \\ 0 & \text{o.w.} \end{cases} \quad (\text{A1})$$

The correlation between the i th atom of molecule a and the j th atom of molecule b is given by

$$\begin{aligned} (\mathbf{R}(\mathbf{x}_a, \mathbf{x}_b))_{ij} &= \nabla_{\mathbf{r}^{ai}} K(\mathbf{D}(\mathbf{x}_a), \mathbf{D}(\mathbf{x}_b)) \nabla_{\mathbf{r}^{bj}}^T \\ &= \sum_{pq=11}^{NN} \sum_{mn=11}^{NN} \frac{\partial^2 K}{\partial \mathbf{D}_{pq} \partial \mathbf{D}_{mn}} \frac{\partial \mathbf{D}(\mathbf{x}_a)_{pq}}{\partial \mathbf{r}^{ai}} \frac{\partial \mathbf{D}(\mathbf{x}_b)_{mn}}{\partial \mathbf{r}^{bj}} \\ &= \begin{cases} \frac{\partial^2 K}{\partial \mathbf{D}_{ij} \partial \mathbf{D}_{ij}} \frac{\partial \mathbf{D}(\mathbf{x}_a)_{ij}}{\partial \mathbf{r}^{ai}} \frac{\partial \mathbf{D}(\mathbf{x}_b)_{ij}}{\partial \mathbf{r}^{bj}} & \text{if } i > j, \\ \frac{\partial^2 K}{\partial \mathbf{D}_{ji} \partial \mathbf{D}_{ji}} \frac{\partial \mathbf{D}(\mathbf{x}_a)_{ji}}{\partial \mathbf{r}^{ai}} \frac{\partial \mathbf{D}(\mathbf{x}_b)_{ji}}{\partial \mathbf{r}^{bj}} & \text{if } i < j, \\ \sum_{p \text{ or } q=i} \sum_{m \text{ or } n=j} \frac{\partial^2 K}{\partial \mathbf{D}_{pq} \partial \mathbf{D}_{mn}} \frac{\partial \mathbf{D}(\mathbf{x}_a)_{pq}}{\partial \mathbf{r}^{ai}} \frac{\partial \mathbf{D}(\mathbf{x}_b)_{mn}}{\partial \mathbf{r}^{bj}} & \text{if } i = j, \end{cases} \end{aligned}$$

where $\frac{\partial^2 K}{\partial \mathbf{D}_{pq} \partial \mathbf{D}_{mn}}$ is the simplified notation of $\frac{\partial^2 K(\mathbf{D}(\mathbf{x}_a), \mathbf{D}(\mathbf{x}_b))}{\partial \mathbf{D}(\mathbf{x}_a)_{pq} \partial \mathbf{D}(\mathbf{x}_b)_{mn}}$.

According to the above equation, when $i = j$, the number of terms in the summation is much larger than the number of terms when $i \neq j$. This mathematical fact indicates that the absolute correlation between different atoms $(\mathbf{R}(\mathbf{x}_a, \mathbf{x}_b))_{ij}$, where $i \neq j$, is typically small compared to the correlation between same atoms $(\mathbf{R}(\mathbf{x}_a, \mathbf{x}_b))_{ii}$. Note that this empirical result typically holds for usual kernel function such as Gaussian kernel and Matérn kernel before enforcing the constraint for permutational symmetry.

The low absolute correlation of force between different atoms does not reflect the permutational symmetries that intrinsically hold for some molecules. The permutational symmetry can be enforced by the PS kernel function from Equ. (4). As shown in e.g. part (a) in Fig. 1 for benzene, after adopting the KS kernel function, the correlation between PE atoms is large due to permutational symmetries, whereas the correlation of force between atoms in different PE atom sets is still small, indicating that we may only need to condition on forces of atoms in the same PE atom set for efficiently calculating the predictive distribution.

Appendix B: Fast Predictions of potential energies in batches

This section discusses the efficient way to calculate the inversion of the covariance matrix in the AFF model on energy prediction. We achieve the reduced computational cost by predicting the molecules' energies in batches rather than the energy for one configuration each time. Let b be the batch size, and $\mathbf{x}^{b*} = [\mathbf{x}_1^*, \dots, \mathbf{x}_b^*]$ be b configurations of a molecular structure. For predicting the energy of a new configuration of this molecular structure, we need to calculate the inversion of Σ_{sub} ,

where $\Sigma_{sub} = \begin{bmatrix} \mathbf{A} & \mathbf{B} \\ \mathbf{C} & \mathbf{D} \end{bmatrix}$, with $\mathbf{A} = \mathbf{K}_{\mathbf{X},\mathbf{X}} + \lambda \mathbf{I}_M$ being a $M \times M$ matrix, $\mathbf{B} = -\mathbf{J}_{\mathbf{X},\mathbf{x}^{b*}}$ being a $M \times 3Nb$ matrix, $\mathbf{C} = -\mathbf{J}_{\mathbf{x}^{b*},\mathbf{X}}$ being a $3Nb \times M$ matrix, and $\mathbf{D} = \mathbf{R}_{\mathbf{x}^{b*},\mathbf{x}^{b*}} + \lambda \mathbf{I}_{3Nb}$ being a $3Nb \times 3Nb$ matrix. Note that the sub-covariance matrix of training energy samples \mathbf{A} is the same among all different batches in prediction. Thus we need to invert \mathbf{A} once and by applying the block matrix inversion for Σ_{sub} , we have:

$$\Sigma_{sub}^{-1} = \begin{bmatrix} \mathbf{A}^{-1} + \mathbf{A}^{-1}\mathbf{B}\mathbf{D}^{*-1}\mathbf{C}\mathbf{A}^{-1} & -\mathbf{A}^{-1}\mathbf{B}\mathbf{D}^{*-1} \\ -\mathbf{D}^{*-1}\mathbf{C}\mathbf{A}^{-1} & \mathbf{D}^{*-1} \end{bmatrix}, \quad (\text{B1})$$

where $\mathbf{D}^* = \mathbf{D} - \mathbf{C}\mathbf{A}^{-1}\mathbf{B}$. Accordingly, for each batch samples, we just need to do a matrix inversion on a $3Nb \times 3Nb$ matrix \mathbf{D}^* , which is much faster than inverting the entire covariance matrix Σ_{sub} for each batch sample.

Appendix C: Predictive distribution of potential energy

To simplify the notation, we would use the batch size $b = 1$ in this section. Conditional on simulated energies in the training dataset \mathbf{E} , and the atomic force $\mathbf{F}(\mathbf{x}^*)$ at the new configuration \mathbf{x}^* , and the estimated parameters $\hat{\boldsymbol{\theta}} = [\hat{m}, \hat{\sigma}^2, \hat{\gamma}, \hat{\lambda}]$, the conditional distribution of the energy at this configuration follows

$$E(\mathbf{x}^*) | \mathbf{E}, \mathbf{F}(\mathbf{x}^*), \hat{\boldsymbol{\theta}} \sim \mathcal{MN}(\mu_E^*(\mathbf{x}^*), \hat{\sigma}^2 K_E^{**}(\mathbf{x}^*, \mathbf{x}^*)), \quad (\text{C1})$$

where the conditional mean follows

$$\mu_E^*(\mathbf{x}^*) = \hat{m} + [\mathbf{K}_{\mathbf{x}^*,\mathbf{X}} - \mathbf{J}_{\mathbf{x}^*,\mathbf{x}^*}^T] \Sigma_{sub}^{-1} \begin{bmatrix} \mathbf{E} - \hat{m} \mathbf{1}_M \\ \mathbf{F}(\mathbf{x}^*) \end{bmatrix},$$

with $\Sigma_{sub} = \begin{bmatrix} \mathbf{K}_{\mathbf{X},\mathbf{X}} & -\mathbf{J}_{\mathbf{X},\mathbf{x}^*} \\ -\mathbf{J}_{\mathbf{x}^*,\mathbf{X}} & \mathbf{R}_{\mathbf{x}^*,\mathbf{x}^*} \end{bmatrix} + \lambda \mathbf{I}_{3N+M}$, and the conditional variance follows

$$\mathbf{K}_E^{**}(\mathbf{x}^*, \mathbf{x}^*) = K_{\mathbf{x}^*,\mathbf{x}^*} - [\mathbf{K}_{\mathbf{x}^*,\mathbf{X}} - \mathbf{J}_{\mathbf{x}^*,\mathbf{x}^*}^T] \Sigma_{sub}^{-1} \begin{bmatrix} \mathbf{K}_{\mathbf{x}^*,\mathbf{X}}^T \\ -\mathbf{J}_{\mathbf{x}^*,\mathbf{x}^*} \end{bmatrix}.$$

Note that we do not observe $\mathbf{F}(\mathbf{x}^*)$ and thus Equ. (C1) cannot be directly used for predicting energy at the new configuration \mathbf{x}^* . Given the energy of training set \mathbf{E} and the atomic force of training set \mathbf{F} , we use the total expectation to integrate the unobserved force vector by its predictive distribution:

$$\begin{aligned} \hat{E}(\mathbf{x}^*) &= \mathbb{E}[E(\mathbf{x}^*) | \mathbf{E}, \mathbf{F}] \\ &= \mathbb{E}[\mathbb{E}[E(\mathbf{x}^*) | \mathbf{E}, \mathbf{F}, \mathbf{F}(\mathbf{x}^*)]] \\ &\doteq \mathbb{E}[\mathbb{E}[E(\mathbf{x}^*) | \mathbf{E}, \mathbf{F}(\mathbf{x}^*)] | \mathbf{F}] \\ &= \mathbb{E}[\mu_E^*(\mathbf{x}^*) | \mathbf{E}, \mathbf{F}], \end{aligned}$$

where \doteq denotes the approximation of $\mathbb{E}[E(\mathbf{x}^*) | \mathbf{E}, \mathbf{F}, \mathbf{F}(\mathbf{x}^*)]$ by $\mathbb{E}[E(\mathbf{x}^*) | \mathbf{E}, \mathbf{F}(\mathbf{x}^*)]$, which is equivalent

to assume that given $(\mathbf{E}, \mathbf{F}(\mathbf{x}^*))$, $E(\mathbf{x}^*)$ is independent of the rest of force vectors in simulated configurations. Plugging the predictive mean $\hat{\mathbf{F}}(\mathbf{x}^*)$ from the above equation to replace $\mathbf{F}(\mathbf{x}^*)$ in $\mu_E^*(\mathbf{x}^*)$, we approximate the predictive mean of energy for $\mathbb{E}[\hat{E}(\mathbf{x}^*) | \mathbf{E}, \mathbf{F}]$ by $\hat{E}(\mathbf{x}^*)$ with the following expression:

$$\hat{E}(\mathbf{x}^*) = \hat{m} + [\mathbf{K}_{\mathbf{x}^*,\mathbf{X}} - \mathbf{J}_{\mathbf{x}^*,\mathbf{x}^*}^T] \Sigma_{sub}^{-1} \begin{bmatrix} \mathbf{E} - \hat{m} \mathbf{1}_M \\ \hat{\mathbf{F}}(\mathbf{x}^*) \end{bmatrix}.$$

The predictive variance in Equ. (12) can be computed by properties of multivariate normal distributions:

$$K_E^*(\mathbf{x}^*, \mathbf{x}^*) = K_{\mathbf{x}^*,\mathbf{x}^*} - [\mathbf{K}_{\mathbf{x}^*,\mathbf{X}} - \mathbf{J}_{\mathbf{x}^*,\mathbf{x}^*}^T] \Sigma_{sub}^{-1} \begin{bmatrix} \mathbf{K}_{\mathbf{x}^*,\mathbf{X}}^T \\ -\mathbf{J}_{\mathbf{x}^*,\mathbf{x}^*} \end{bmatrix}.$$

Let \mathbf{W}_1 and \mathbf{W}_2 be the first $1 \times M$ block matrix and the latter $1 \times 3N$ block matrix of $[\mathbf{K}_{\mathbf{x}^*,\mathbf{X}} - \mathbf{J}_{\mathbf{x}^*,\mathbf{x}^*}^T] \Sigma_{sub}^{-1}$, respectively, and $\hat{\mathbf{F}}(\mathbf{x}^*) = \boldsymbol{\omega}_F \mathbf{F}$, where $\boldsymbol{\omega}_F$ follows from Equ. (5). We can also write the $\hat{E}(\mathbf{x}^*)$ as the weighted average value of \mathbf{E} and $\hat{\mathbf{F}}(\mathbf{x}^*)$:

$$\hat{E}(\mathbf{x}^*) = \boldsymbol{\omega}_E^* \mathbf{E} + \boldsymbol{\omega}_F^* \mathbf{F}, \quad (\text{C2})$$

where

$$\boldsymbol{\omega}_E^* = (1 - \mathbf{W}_1 \mathbf{1}_M) (\mathbf{1}_M^T \mathbf{K}_{\mathbf{X},\mathbf{X}}^{-1} \mathbf{1}_M)^{-1} \mathbf{1}_M^T K_{\mathbf{X},\mathbf{X}}^{-1} + \mathbf{W}_1,$$

and $\boldsymbol{\omega}_F^* = \mathbf{W}_2 \boldsymbol{\omega}_F$.

Appendix D: Simulation details

In addition to molecules available from the MD17 dataset, force and energy of additional molecules with more atoms and complicated structure are generated in this work. *ab initio* MD (AIMD) simulation is performed via Q-Chem to generate highly accurate molecular force and energy to benchmark AFF and other machine learning force field. In this work, all AIMD simulations are carried in NVT ensemble with timestep of 1 fs at room temperature (300 K). All the calculations were performed at the level of Perdew-Burke-Ernzerhof(PBE)/6-31G(d,p). vdW interactions are taken into account by using TS-vdW method. The Nosé-Hoover thermostat is used to control the temperature.

Appendix E: Timings

All timings were performed on a compute cluster equipped with Intel 6148 CPUs (20 cores each) with a high speed OmniPath interconnect. The compute nodes consist of 64 nodes of 40 core/192GB of RAM compute systems, 4 nodes with 768GB of RAM plus 300 GB Intel Optane Memory Drive, and 3 GPU nodes with four NVIDIA V100/32GB GPUs with NVLINK.